Raman, SERS, and DFT Analysis of the Main Alkaloids Contained in Syrian Rue

María Vega Cañamares[1], Federica Pozzi[2], John R. Lombardi[3]*

[1]Instituto de Estructura de la Materia, Consejo Superior de Investigaciones Científicas (IEM-CSIC), Serrano 121, 28006 Madrid, Spain

[2]Department of Scientific Research, The Metropolitan Museum of Art, 1000 Fifth Avenue, New York, NY 10028, United States

[3]Department of Chemistry, City College of the City University of New York, 160 Convent Ave, New York, NY 10031, United States

Corresponding Author:

María Vega Cañamares

Instituto de Estructura de la Materia,

Consejo Superior de Investigaciones Científicas (IEM-CSIC)

Serrano 121, 28006 Madrid, Spain

Email: mvca@iem.cfmac.csic.es

ABSTRACT

Syrian Rue, obtained from the seeds of the *Peganum Harmala* plant, is a reddish colorant especially popular for dyeing carpets and wool fabrics in Western Asia and traditionally used as an alternative source for the madder-derived dye Turkey Red. The main constituents of the Syrian Rue dye are harmalol, harmaline, harmane, and harmine, which belong to a group of substances collectively known as harmala alkaloids. These compounds are also called β-carboline alkaloids, as they display very similar molecular structures that consist of either a pyridine ring or a nitrogen-containing six-atom ring with two conjugated double bonds, each fused to an indole skeleton. In the present study, Density Functional Theory (DFT) was employed to perform a vibrational analysis of the four constituents of Syrian Rue by means of the Gaussian Package. First, the molecular geometry of each compound was optimized and its Raman spectrum calculated. Then, all the observed Raman bands were assigned to specific vibrational normal modes of the corresponding molecule. As a final step, the FT-Raman and SERS spectra of the four structurally related alkaloids were examined and compared, with the ultimate aim to study the adsorption mechanism of these molecules on silver nanoparticles used as SERS substrates.

INTRODUCTION

The *Peganum Harmala* plant, native to Africa and the Middle East all the way to India, has been employed since ancient times in sacred rituals and traditional medicine. To the present day, possible applications of its main alkaloid constituents to the fields of fertility, as well as antibacterial, anti-protozoal, and antitumor activity are being investigated. In addition, extraction of the *Peganum Harmala* seeds yields a red colorant called Syrian Rue that has found common use to dye carpets and was historically employed as an alternative source for Turkey Red, typically obtained from the roots of the madder plant. While being native to the Mediterranean region and Southern Asia, *Peganum Harmala* was reportedly planted in the United States in 1928 by a farmer in New Mexico wanting to produce a Turkey Red dye for wool yarns[1]. The Syrian Rue dye is composed of four main alkaloids, namely harmalol, harmaline, harmane, and harmine, which belong to a group of substances collectively known as harmala or β-carboline alkaloids and whose closely related structures are reported in Figure 1. Harmane and harmine consist of a pyridine ring fused to an indole skeleton. While the first presents the simplest molecular structure, with a methyl group on the pyridine ring in ortho position to the nitrogen, or 13 in our numbering, the latter has an additional methoxy substituent in position 8. Thus, these two alkaloids are completely planar. On the other hand, in harmalol and harmaline, the indole moiety is combined with a nitrogen-containing six-atom ring displaying two conjugated double bonds, which explains the deviation from planarity of such compounds. Position 8 in harmalol and harmaline is substituted with hydroxyl and methoxy functional groups, respectively.

Surface-enhanced Raman spectroscopy (SERS) has proven to be an invaluable resource for the detection and identification of organic substances in trace levels, such as pesticides, explosives, and drugs[2-4]. Briefly, the adsorption of an organic molecule onto a roughened metal surface results

in an extremely significant enhancement of the Raman scattering, accompanied by a remarkable quenching of the fluorescence emission[5]. This leads to ultrahigh sensitivity compared to normal Raman and, therefore, to the possibility of analyzing minute samples successfully. In the past fifteen years, this technique has also seen increasing application in the cultural heritage field for the characterization of dyes and lake pigments derived from plants and insects or artificially synthesized in a chemical laboratory[6-10]. Scientific analysis of such materials is of great interest to art historians and curators, as information regarding their availability and use in certain time periods and geographical areas may offer insight into the lifestyle and technical knowledge reached by various populations in a given historical age, the trade routes and commercial transactions involved in the creation of an object, as well as the interaction among different cultures. Revealing the nature and origin of dyes and pigments found in artworks may also provide clues as to their intended color and appearance, resulting in an improved understanding of the artist's original intentions and choices. Moreover, from a conservation standpoint, conclusive identification of the paint materials in artifacts of archaeological, historical, and artistic significance may contribute to an informed assessment of their degree of deterioration and to the development of suitable preservation and restoration treatments. A previous study by some of the authors aimed to evaluate the coupling of SERS with thin-layer chromatography (TLC) to resolve complex mixtures of organic colorants[11]. In such work, the main alkaloid constituents of the Syrian Rue dye, as extracted from *Peganum Harmala* seeds, were employed as test molecules. In addition to exploring the capabilities of TLC-SERS, the study in question had provided a comprehensive spectral characterization of the *Peganum Harmala* seed extract along with its individual constituents. In detail, FT-Raman, Raman, and SERS spectra of these compounds acquired at 488, 633, 785, and 1064 nm were reported, and a series of characteristic bands was highlighted for each molecule to

enable conclusive differentiation within identification studies. It should be pointed out that the molecular structures of harmane and harmine shown in the article above mentioned, drawn from a reference book of natural dyes[12], were incorrect; however, this did not affect in any way the validity of the experimental results described.

In the present work, intended as a necessary continuation of the authors previous research, Density Functional Theory (DFT) was employed to perform a vibrational analysis of harmalol, harmaline, harmane, and harmine with the final aim to study the interaction of each of these molecules with a silver surface that may be used within SERS experiments. The molecular orientation of the analytes under examination with respect to the SERS-active substrate plays a key role in determining the extent of the enhancement and the normal modes observed in the molecules' enhanced spectra; as a result, this piece of information greatly contributes to an improved understanding of the SERS mechanism that goes far beyond mere identification of unknowns by qualitative comparison with empirically developed spectral libraries. A similar research was previously carried out to assess the SERS adsorption mechanism of mauve, the first synthetic dye, and its main components on a silver surface[13] upon separation by TLC[14]. Initially, the theoretical Raman spectra were calculated, upon optimization of the compounds molecular geometry, using a B3LYP hybrid exchange correlation functional in combination with a 6-31+G** basis set. Then, a detailed comparison of all the calculated Raman bands with those detected in the experimental spectra was carried out, and the bands were assigned to specific vibrational normal modes of the corresponding molecules. As a final step, the FT-Raman and SERS spectra of the four structurally related alkaloids found in Syrian Rue were examined and carefully compared in order to elucidate the adsorption mechanism of such compounds on the SERS-active silver substrate.

EXPERIMENTAL AND THEORETICAL METHODS

Materials. Silver nitrate, sodium citrate, sulfuric acid, and glucose were obtained from Fisher Scientific, while harmalol, harmaline, harmane, harmine, ethanol, and potassium nitrate (KNO_3) from Sigma-Aldrich. All aqueous solutions used for the silver colloid synthesis were prepared using 18 MΩ ultrapure water (Millipore Simplicity 185 water purification system).

Ag colloid synthesis, sample preparation, and SERS analysis. Silver colloids for SERS were synthesized by microwave-supported glucose reduction of silver sulfate in the presence of sodium citrate as a capping agent, according to a previously published method[15]. Reference solutions of harmalol, harmaline, harmane, and harmine were prepared in ethanol at a concentration of 10^{-4} M. For SERS analysis, 0.2 μL of the analyte solution and 0.1 μL of a 0.5M KNO_3 aqueous solution were added in sequence to 0.8 μL of the Ag colloid. SERS measurements were then performed by focusing the laser beam just below the surface of the silver microaggregates that became visible upon aggregation in the colloid-analyte droplet.

Instrumentation. FT-Raman spectra of the four alkaloids were acquired with a Bruker RamII Vertex 70 spectrometer equipped with a liquid nitrogen-cooled Ge detector. The 1064 nm line provided by a Nd:YAG laser was used for excitation, with a resolution of 4 cm^{-1} and a 180 degrees geometry. FT-Raman measurements were taken by collecting 128 scans and using a 25 mW output laser power. SERS spectra were recorded with the Bruker Senterra Raman instrument mentioned above, using a 20x long working distance microscope objective and excitation at 488 nm, with a single integration of 30 s.

DFT calculations. For all the alkaloid molecules examined in the present work, optimization of the ground state neutral singlet structures and calculation of the theoretical Raman spectra were

performed with DFT using the Gaussian 09 package[16]. All the calculations were performed in vacuum conditions, using a B3LYP hybrid exchange correlation functional in combination with 6-31G** as a basis set. Upon optimization of the molecular geometry, Raman spectra were obtained; no imaginary wavenumbers were observed in the calculated spectra. GaussView 5.09 was employed to view data and output images. Detailed assignments of the vibrational normal modes were based on the best fit comparison of the wavenumbers of calculated and experimental Raman bands.

The DFT calculations are carried out assuming the molecule is isolated (i.e., in the gas phase) while the FT-Raman spectra are taken in the powder (or crystalline) form, and therefore some differences in the intensities as well as the frequencies of some of the lines were expected. Shits from the experimental bands are also observed due to neglecting the anharmonicity effects in the theoretical treatment. A slight drift of the deviation with increasing wavenumber is expected because of higher errors in correlation corrections. Scaling factors[17] are commonly used in the calculated spectra in order to correct the correlation effects that are only partially accounted for in DFT; in this work, 0.97 and 0.99 were used as scaling factors in spectral regions above and below 1100 and 1200 cm^{-1} for harmane/harmine and harmaline/harmalol, respectively. Given these expected shifts, the results obtained are considered to be in close agreement.

RESULTS AND DISCUSSION

FT-Raman spectrum, DFT calculations, and normal mode assignments. Optimized geometries of the harmala alkaloids are shown in Figure S1. As it was expected, harmane and harmine have a mainly planar structure formed by the three aromatic rings. On the other hand, the

plane of harmaline and harmalol is only formed by rings I and II, as ring III is not aromatic and the conjugation along the molecules is broken.

Figure 2a shows the FT-Raman and DFT spectra of harmane. The main Raman bands appear at 1627, 1577, 1484, 1405, 1322, 1305, 1284, 1237, 1110, 1012, 978, 884, 712, 520, 450 and 312 cm^{-1}. Avery good fit was obtained between the experimental and calculated spectra of harmane, not only in the wavenumbers but also in the intensity of the bands. This clearly indicates the suitability of the level of theory used and an appropriate selection of basis set for this molecule. Assignments of harmane vibrational normal modes derived from the calculations are shown in Table 1. On the one hand, assignment of the benzene normal modes was performed for the three aromatic rings. Two different notations were used: the Gardner and Wright correlations for monosubstituted benzenes which has proven quite valuable in vibrational spectroscopy studies[18] and the well-established Wilson notation for benzene modes[19]. On the other hand, the normal modes for the rest of the molecule were assigned separately. The most intense Raman band of harmane, at 1322 cm^{-1}, is assigned to the δ(CH) of the pyridine ring III and to the stretching of the benzene ring I, ν_I(ring). Other intense bands at 1627 and 1577 cm^{-1} are assigned to the ν_I(ring) as well. Several bands in the region 1510-1200 cm^{-1}, such as those at 1505, 1412, 1380, 1284, 1237 and 1218 cm^{-1}, are attributed to ν(N11C) in ring II, in some cases together with benzene and pyridine rings vibrations. The medium intensity bands at 1012, 884 and 712 cm^{-1} are associated to in-plane bending vibrations δ(CH), δ(ring) and δ(N11C). The most intense band assigned to an out-of-plane deformation, γ_I(ring), is observed at 450 cm^{-1}.

A comparison of the experimental and calculated Raman spectra of harmine is presented in Figure 2b. A list of the main bands observed in the spectra is given in Table 2, along with the assignment of the corresponding vibrational normal modes. As the only difference in the molecular

structures of harmane and harmine is the presence of an -OCH_3 in position 8 for the latter, it is reasonable that the FT-Raman spectra of these two alkaloid compounds are also analogous. The main bands are observed at 1629, 1575, 1486, 1417, 1341, 1326, 1291, 1237, 1101, 977, 875, 776, 676, 528 and 298 cm^{-1}. The DFT calculated spectrum also shows a very good fit with the experimental one. The main differences in the assignment of the vibrational normal modes are ascribable to the ether group. Thus, medium intensity bands at 776 and 676 cm^{-1} are associated to δ(COC). This vibration is also assigned to weak bands at 570 and 501 cm^{-1}. Stretching vibrations of -OCH_3 correspond to low intensity bands at 1214 and 1185 cm^{-1}. Finally, the out-of-plane deformation is found at 1166 cm^{-1}.

Figure 3a shows the FT-Raman and the DFT calculated spectra of harmaline. The main FT-Raman bands are observed at 1625, 1540, 1471, 1438, 1372, 1301, 1071, 980, 857 and 761 cm^{-1}. When compared to the Raman spectra of harmine, many differences can be noticed, both in terms of wavenumber and intensity of the bands. Despite the overall similarity of the harmaline and harmine molecular structures, the lack of aromaticity of the former in ring III gives rise to a change in the planarity and, therefore, a change in the molecular symmetry. The calculated spectrum shows a very good fit with the experimental one. However, the wavenumbers of the bands assigned to ν(C=N), at 1625 and 1604 cm^{-1}, appear at higher values in the calculated spectrum (table 3). The same phenomenon is also encountered when considering the ν(C_4=C_{12}) normal mode at 1540 cm^{-1}. Bands at 1471 and 1372 cm^{-1} correspond to δ($C_{15}H_3$) and δ($C_{14}H_3$), respectively. Other distinctive normal modes are those associated to stretching vibrations of C_4-C_5, C_{12}-C_{13}, N_1-C_2 and C_3-C_2 at 1301, 1273, 1071 and 980/857 cm^{-1}, respectively.

A comparison between the experimental and calculated Raman spectra of harmalol is shown in Figure 3b. The main FT-Raman bands are observed at 1635, 1559, 1442, 1376, 1340, 1295, 1260,

1079, 996, 859, 776, 655 and 624 cm^{-1}. DFT and FT-Raman spectra show an overall good correspondence except for the 1400-1100 cm^{-1} region, where both the wavenumbers and the intensities of the bands appear rather different. Even though harmalol and harmaline only differ in the substituent on the benzene ring, when their FT-Raman spectra are compared several differences may be appreciated. The main changes are observed in the relative intensity of the bands at 1559/1340 and 1540/1372 cm^{-1} in harmalol and harmaline, respectively, although they are assigned to the same modes, $\nu(C4{=}C12)/\delta_w(CH_2)$ (Tables 3 and 4). The most intense Raman bands are associated to aromatic rings, C=C, C=N, CH, CH_2 and CH_3 vibrations as observed in Table 4. However, the majority of the least intense Raman bands are attributed to vibrational normal modes of the hydroxyl group. Thus, bands at 1517, 1403, 1195, 1180 and 1141 cm^{-1} are assigned to δ(OH) and those at 1517, 1312, 1260, 1195 and 776 cm^{-1} correspond to ν(CO).

SERS spectra and adsorption mechanisms. Figure 4a presents a comparison between the experimental SERS and FT-Raman spectra of harmane. The main bands appear at 1626, 1579, 1455, 1374, 1329, 1236, 1011, 978, 914, 881, 719, 642 and 590 cm^{-1}. The observation of the differences in the position and intensity of the bands of the normal Raman and SERS spectra enables to deduct the adsorption mechanism of the molecule on the Ag surface. In the case of harmala alkaloids, there are two possible adoption geometries: perpendicular to the metallic surface, through the lone pair of electrons of one nitrogen atom in ring II or III; or parallel to the Ag along the plane formed by the aromatic rings. Little differences are observed between the FT-Raman and SERS spectra of harmane. No great shifts are seen in the wavenumber of the bands of harmane. However, regarding the intensity, enhancements of the bands at 1626, 1455, 1374 and 1236 cm^{-1} are observed in the SERS spectra (Figure 4Ia). As shown in Table 1, these bands are assigned to ν_I(ring), ν_I(ring)/$\delta(CH_3)$, $\nu(N11C)/\nu_I$(ring) and$\nu(N11C)/\delta_I$(CH), respectively. All of

these are in-plane vibrations. Thus, according to the SERS selection rules[20] a perpendicular adsorption geometry is deduced. In addition, most of the bands assigned to the pyridine ring, such as those at 1566, 1481, 1398, 1304, 1220 and 457 cm^{-1}, are subject to a decrease in intensity in the SERS spectra. This can be due to the proximity of ring III to the Ag surface, suggesting an interaction through the pyridine nitrogen atom. The presence of the methyl group in the ortho position with respect to the N can cause the molecule to be tilted on the metal surface, instead of being totally perpendicular, as it was deduced in another work for 2-methylpyridine[21]. Indeed, methyl groups are rather bulky and, if they are adjacent to the N atom interacting with the Ag surface, they could affect the molecule-metal interaction by steric hindrance[22]. There would be a distortion of the methyl by proximity of the surface, leading to interaction of the group with the Ag. As no changes in the wavenumbers of the bands assigned to $-CH_3$ were observed, the molecule should be tilted away from that substituent (Figure 5).

Figure 4b shows the FT-Raman and SERS spectra of harmine. The main SERS bands are observed at 1635, 1568, 1441, 1346, 1297, 1258, 1238, 1221, 977, 951, 881, 775, 676 and 660 cm^{-1}. As in the case of harmane, most SERS bands show little or no shifts compared to the FT-Raman spectrum. However, several changes in the relative intensities are observed. Harmine bands at 1441, 1258, 1221, 951, 924, and 663 cm^{-1} are enhanced on the Ag surface. Most of these bands are assigned to in-plane vibrations, suggesting, again, a perpendicular orientation of this alkaloid on the metal nanoparticles. Additionally, the SERS bands at 1568, 1484, 1415, 1297, 1109 and 811 cm^{-1}, assigned to normal modes of the pyridine ring, have lower intensity in comparison to the FT-Raman bands. Thus, harmine interacts with the Ag in the same way as harmane, through the N of the pyridine ring, in a slightly tilted position with respect to the metal surface (Figure 5).

The comparison of the SERS and FT-Raman spectra of harmaline is shown in Figure 4c. The main SERS bands are located at 1629, 1599, 1542, 1465, 1372, 1335, 1171, 1076, 989, 770, 654 and 617 cm^{-1}. Many changes in the intensity of the bands are observed, such as a great enhancement of bands at 1629, 1599, 1568, 1335, 1313 and 617 cm^{-1} in the SERS spectrum. As shown in Table 3, the vibrational normal modes assigned to these bands are ν(C=N), ν(C=N)/ν_I(ring), ν_I(ring), ν_I(ring)/δ(CH_2)/ν(N11C), ν(C4-C5)/δ_{tw}(C_2H_2) and δ(COC)/δ_{III}(ring)/ν(C-CH_3), respectively. A significant decrease of the intensity of the SERS bands is observed at 1542 and 1465 cm^{-1}, associated to ν(C4=C12) and δ($C_{15}H_3$). All the observed changes are related to in-plane normal modes. If the interaction between harmaline and Ag takes place through the pyridine nitrogen in a tilted geometry with respect to the surface, the C=N and C4=C12 bonds will be perpendicular and parallel to the surface, respectively (Figure 5). Thus, the stretching vibrations of those bonds will have the same orientation on the Ag. According to the SERS selection rules, the intensity of the bands associated to those normal modes will be increased and decreased respectively, as it was observed in the SERS spectrum of harmaline.

The SERS spectrum of harmalol is shown in Figure 6 together with the FT-Raman spectrum. The most intense SERS bands appear at 1615, 1600, 1556, 1486, 1442, 1324, 1076, 986 and 617 cm^{-1}. In the case of this harmala alkaloid not only are differences observed in the intensity of the bands, but also in the wavenumbers. This suggests a different adoption mechanism of harmalol and harmaline, despite of the small differences in the molecular structure. The hydroxyl group in position 8 in ring I could deprotonate in contact with the Ag surface, so the interaction with Ag could take place perpendicular via the oxygen atom. To confirm this hypothesis, a decrease of the SERS bands assigned to O-H vibrations, such as those at 1600, 1514, 1410, 1190, 1174 and 1137 cm^{-1}, should be observed (Table 4). However, the intensity decrease of those bands is notseen.

Therefore, a perpendicular interaction of harmalol through the OH group in ring I can be ruled out. A very important change in the SERS spectra is the shift of the FT-Raman band at 1635 to 1615 cm^{-1}. This is assigned to ν(C=N) and ν(C_4=C_{12}) (Table 4). This shift towards lower wavenumbers is related to a decrease in the strength of both double bonds suggesting a parallel orientation of the alkaloid with respect to the Ag surface or to a parallel stacking of various harmalol molecules. The great enhancement of the SERS band at 617 cm^{-1}, assigned to out-of-plane deformations of ring I and the NH group (Table 4), supports the parallel interaction of the alkaloid on the Ag surface. The interaction would take place through both the oxygen atom in the benzene ring and the nitrogen in the pyridine ring (Figure 7).

CONCLUSIONS

In this work, harmalol, harmaline, harmane, and harmine have been subjected to a detailed vibrational analysis involving experimental FT-Raman spectroscopy and SERS, as well as theoretical calculations by DFT. First, the molecular geometry of each compound was optimized and its Raman spectrum calculated using a B3LYP hybrid exchange correlation functional in combination with a 6-31+G** basis set. Then, the results of the calculations were compared with experimental FT-Raman spectra, and all the observed Raman bands were successfully assigned to specific vibrational normal modes of the corresponding molecule. As a final step, the experimental SERS and FT-Raman spectra of the four structurally related alkaloids were examined and compared. SERS selection rules were applied in order to deduce the adsorption mechanism of the alkaloids on the silver surface. Results have shown that harmaline, harmane, and harmine may adopt an adsorption geometry that is perpendicular and slightly tilted with respect to the silver, in which interaction with the metal surface takes place through the nitrogen atom of the pyridine ring;

on the other hand, despite its overall structural similarity with harmaline, harmalol lies parallel to the silver, with which it likely interacts through the nitrogen atom of the pyridine ring and the hydroxyl group of ring I. The detection of differences in the FT-Raman and SERS spectra of harmalol clearly demonstrates the crucial role played by surface effects on the acquisition of data and prompts the analyst to a greater awareness of the spectral changes that might be expected upon adsorption of the molecule onto a metal surface and ring substitution, among other factors. Special attention in this regard must be paid when examining spectra for evidence of chemical degradation and in all other instances in which a more detailed analysis of the SERS data is to be performed.

ASSOCIATED CONTENT

Supporting Information

The following file is available free of charge:

Figure S1. Optimized structures of (a) harmane, (b) harmine, (c) harmaline and (d) harmalol.

AUTHOR INFORMATION

Corresponding Author

* Email: mvca@iem.cfmac.csic.es

Author Contributions

The manuscript was written through contributions of all authors. All authors have given approval to the final version of the manuscript.

ACKNOWLEDGMENTS

This research was supported by CSIC (Spanish National Research Council) through I-link+ Internalization Program (project i-link1148) and Ministerio de Economía, Industria y Competitividad de España (project FIS2017-84318-R). We are also indebted to the National Science Foundation (CHE-1041832)

REFERENCES

[1] J. Davison, M. Wargo, Recognition and Control of African Rue in Nevada, University of Nevada, Reno, 2001.

[2] P. H. B. Aoki, L. N. Furini, P. Alessio, A. E. Aliaga, C. J. L. Constantino, Surface-enhanced Raman scattering (SERS) applied to cancer diagnosis and detection of pesticides, explosives, and drugs. Rev. Anal. Chem. 2013; 32(1), 55.

[3] C. Muehlethaler, M. Leona, J. R. Lombardi, Review of surface enhanced Raman scattering applications in forensic science. Anal. Chem. 2016; 88(1), 152.

[4] V. Rana, M. V. Cañamares, T. Kubic, M. Leona, J. R. Lombardi, Surface-Enhanced Raman Spectroscopy for Trace Identification of Controlled Substances: Morphine, Codeine, and Hydrocodone. J. Forensic Sci. 2011; 56(1), 200.

[5] M. Moskovits, Surface-enhanced spectroscopy. Rev. Mod. Phys. 1985; 57, 783.

[6] F. Casadio, M. Leona, J. R. Lombardi, R. P. Van Duyne, Identification of organic colorants in fibers, paints, and glazes by surface enhanced Raman spectroscopy. Acc. Chem. Res. 2010; 43(6), 782.

[7] F. Pozzi and M. Leona, Surface-enhanced Raman spectroscopy in art and archaeology. J. Raman Spectrosc. 2016; 47(1), 67.

[8] F. Pozzi, S. Zaleski, F. Casadio, M. Leona, J. R. Lombardi, R. P. Van Duyne, Surface-enhanced Raman spectroscopy: using nanoparticles to detect trace amounts of colorants in works of art. In Nanoscience and Cultural Heritage, Eds. Ph. Dillmann, L. Bellot-Gurlet, I. Nenner, Atlantis Press, 2016, pp. 161-204.

[9] M. V. Cañamares, M. Leona, M. Bouchard, C. M. Grzywacz, J. Wouters, K. Trentelman, Evaluation of Raman and SERS Analytical Protocols in the Analysis of Cape Jasmine Dye (*Gardenia Augusta* L.). J. Raman Spectrosc. 2010; 41, 391.

[10] I. Bonacini, F. Gallazzi, A. Espina, M. V. Cañamares, S. Prati, R. Mazzeo, S. Sanchez-Cortes, Sensitive 'on the fiber' detection of synthetic organic dyes by laser photoinduced plasmonic Ag nanoparticles, J. Raman Spectrosc. 2017; 48(7), 925.

[11] F. Pozzi, N. Shibayama, M. Leona, J. R. Lombardi, TLC-SERS study of Syrian rue (*Peganum harmala*) and its main alkaloid constituents. J. Raman Spectrosc. 2013; 44(1), 102.

[12] H. Schweppe, Handbuch der Naturfarbstoffe, Landsberg/Lech, Germany, 1993.

[13] M. V. Cañamares, J. R. Lombardi, Raman, SERS, and DFT of Mauve Dye: Adsorption on Ag Nanoparticles. J. Phys. Chem C 2015; 119, 14297.

[14] M. V. Cañamares, D. A. Reagan, J. R. Lombardi, M. Leona, TLC-SERS of mauve, the first synthetic dye. J. Raman Spectrosc. 2014; 45(11-12), 1147.

[15] M. Leona, Microanalysis of organic pigments and glazes in polychrome works of art by surface-enhanced resonance Raman scattering. Proc. Natl. Acad. Sci. 2009; 106, 14757.

[16] Gaussian 09, Revision A.02, M. J. Frisch, G. W. Trucks, H. B. Schlegel, G. E. Scuseria, M. A. Robb, J. R. Cheeseman, G. Scalmani, V. Barone, G. A. Petersson, H. Nakatsuji, X. Li, M. Caricato, A. Marenich, J. Bloino, B. G. Janesko, R. Gomperts, B. Mennucci, H. P. Hratchian, J.

V. Ortiz, A. F. Izmaylov, J. L. Sonnenberg, D. Williams-Young, F. Ding, F. Lipparini, F. Egidi, J. Goings, B. Peng, A. Petrone, T. Henderson, D. Ranasinghe, V. G. Zakrzewski, J. Gao, N. Rega, G. Zheng, W. Liang, M. Hada, M. Ehara, K. Toyota, R. Fukuda, J. Hasegawa, M. Ishida, T. Nakajima, Y. Honda, O. Kitao, H. Nakai, T. Vreven, K. Throssell, J. A. Montgomery, Jr., J. E. Peralta, F. Ogliaro, M. Bearpark, J. J. Heyd, E. Brothers, K. N. Kudin, V. N. Staroverov, T. Keith, R. Kobayashi, J. Normand, K. Raghavachari, A. Rendell, J. C. Burant, S. S. Iyengar, J. Tomasi, M. Cossi, J. M. Millam, M. Klene, C. Adamo, R. Cammi, J. W. Ochterski, R. L. Martin, K. Morokuma, O. Farkas, J. B. Foresman, and D. J. Fox, Gaussian, Inc., Wallingford CT, 2016.

[17] J. P. Merrick, D. Moran, L. Radom, An evaluation of harmonic vibrational frequency scale factors. J. Phys. Chem. A 2007; 111, 11683-1700.

[18] A. M. Gardner, T. G. Wright, Consistent assignment of the vibrations of monosubstituted benzenes. J. Chem. Phys. 2011; 135(11), 114305.

[19] E. B. Wilson Jr., The normal modes and frequencies of vibration of the regular plane hexagon model of the benzene molecule. Phys. Rev. 1934; 45(10), 706.

[20] J. R. Lombardi, R. L. Birke, A unified approach to surface-enhanced Raman spectroscopy. J. Phys. Chem. C 2008; 112(14), 5605.

[21] K. A. Bunding, J. R. Lombardi, R. L. Birke, Surface enhanced Raman spectra of methylpyridines. Chem. Phys. 1980; 49, 53.

[22] K. A. Bunding, R. L. Birke, J. R. Lombardi, The surface enhanced Raman spectrum of 2,6-lutidine. Chem. Phys. 1980; 54, 115.

TOC Graphic

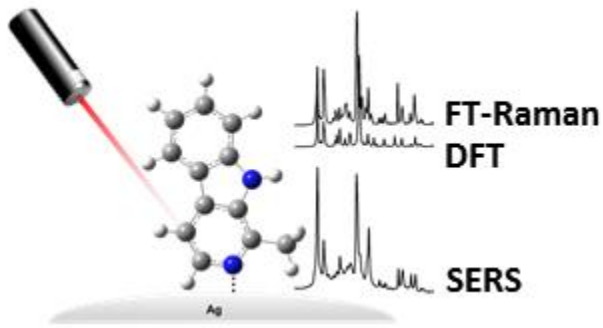

Tables

Table 1. Main experimental and calculated Raman wavenumbers (cm^{-1}) of harmane and assignments derived from the DFT calculations (B3LYP/6-31G**).

Raman wavenumber[a] / cm^{-1}			Assignments[b]		
SERS	FT-Raman	DFT (scaled)	Benzene modes		Other modes
			Gardner	Wilson	
1626 vs	1627 m	1625	$\mathcal{M}_4$	9a (I)	
1603 sh	1604 vw	1600	$\mathcal{M}_4$	9a (III)	
1579 m	1577 m	1578	$\mathcal{M}_{23}$	9b (I)	
1566 sh	1567 sh	1571	$\mathcal{M}_{23}$	9b (III)	
1503 w	1505 vw	1493	$\mathcal{M}_5$	18a (I)	ν(N11C)
1481 w	1484 w	1478	$\mathcal{M}_5$	18a (III)	$\delta_{as}(CH_3)$
1455 m	1455 w	1455	$\mathcal{M}_{24}$	18b (I)	$\delta_{as}(CH_3)$
1398 w	1412 sh 1405 w	1414	$\mathcal{M}_{24}$	18b (III)	ν(N11C)/$\delta_{as}(CH_3)$
1374 m-w	1380 w	1379			ν(N11C)/ν_I(ring)
	1365 sh	1373			$\delta_s(CH_3)$
1329 vs	1322 s	1311	$\mathcal{M}_{26}$	3 (III)	ν_I(ring)
1304 sh	1305 m-s	1302	$\mathcal{M}_{26}$/ $\mathcal{M}_{25}$	3 (I)/15 (III)	
1284 sh	1284 m-w	1264			ν(N11C)/δ(CH)/ν(C-CH_3)
1247 sh	1257 w	1240			ν_{III}(ring)
1236 s	1237 m-w	1227			ν(N11C)/δ_I(CH)
1220 sh	1218 w	1194	$\mathcal{M}_7$	8a (III)	ν(N11C)/δ_I(CH)
1154 w	1154 vw	1172	$\mathcal{M}_{27}$	14 (I)	
1133 vw	1133 vw	1139			δ_I(CH)
1110 w	1110 w	1116			δ(NH)/$\rho(CH_3)$/δ(CH)
1074 vw	1071 vw	1083	$\mathcal{M}_{28}$	19b (III)	δ(N11C)/δ_I(ring)
	1042 vw	1045			$\delta_{as}(CH_3)$
1011 m	1012 m	1034	$\mathcal{M}_8$	19a (I)	
978 m	978 w	981			$\rho(CH_3)$
	940 vw	948	$\mathcal{M}_{12}$	17a (III)	
914 m	915 w	912	$\mathcal{M}_9$	12 (I)	δ(N11C)/ν(C-CH_3)/δ_{III}(ring)
881 m	884 m	878			δ(N11C)/δ_{III}(ring)
	848 vw	854	$\mathcal{M}_{16}$	10b (I)	
838 vw	836 vw	842			δ(N11C)/$\delta_{I,III}$(ring)
822 vw	822 vw	834	$\mathcal{M}_{13}$	10a (III)	
	753 vw	755			γ_I(CH)
719 m-s	712 m	721			δ(ring)

637 sh	636 vw	639	$\mathcal{M}_{29}$	6b (I)	δ_{III}(ring)
598 sh	599 sh	609			γ(ring)
590 w	589 vw	589	$\mathcal{M}_{11}$	6a (III)	δ_{I}(ring)
564 vw	566 vw	561			$\delta_{I,III}$(ring)
517 vw	520 w	519			$\delta_{I,III}$(ring)/δ(C-CH_3)
457 vw	450 w	440	$\mathcal{M}_{19}$	16b (I)	
	327 sh	360			
320 vw	312 w	299		Skeletal vibrations	
	300 w	289			

[a] vw, very weak; w, weak; m, medium; s, strong; vs, very strong; sh, shoulder.

[b] ν, stretching; δ, in-plane bending; δ_{tw}, twist deformation; δ_{sc}, scissoring deformation; δ_{w}, wag deformation; γ, out-of-plane bending; ρ, rocking; s, symmetric; as, antisymmetric.

Table 2. Main experimental and calculated Raman wavenumbers (cm^{-1}) of harmine and assignments derived from the DFT calculations (B3LYP/6-31G**).

Raman wavenumber[a] / cm^{-1}			Assignments[b]		
SERS	FT-Raman	DFT (scaled)	Benzene modes		Other modes
			Gardner	Wilson	
1635 s	1629 m-s	1636	$\mathcal{M}_4$	9a (I)	
1568 m	1575 m	1601	$\mathcal{M}_4$	9a (III)	
1541 sh	1546 vw	1571	$\mathcal{M}_{23}$	9b (I)	
	1513 vw	1507	$\mathcal{M}_5$	18a (I)	$\nu_{as}(N11C)/\delta_s(C15H_3)$
1484 vw	1486 w	1478	$\mathcal{M}_5$	18a (III)	$\delta_{as}(C14H_3)$
1466 sh	1459 vw	1459			$\delta_{as}(C15H_3)/\delta_s(C15H_3)$
1441 w	1446 vw	1439	$\mathcal{M}_{24}$	18b (I)	$\delta_s(C15H_3)$
1415 vw	1417 w	1414	$\mathcal{M}_{24}$	18b (III)	$\delta_{as}(C14H_3)$
1384 sh	1390 w	1372			$\delta_s(C14H_3)$
1346 s	1341 s	1358			$\nu_{as}(N11C)/\nu_I(ring)$
1331 sh	1326 sh	1314	$\mathcal{M}_{26}$	3 (III)	$\nu_{as}(N11C)/\nu_I(ring)$
1297 m	1291 m-s	1294	$\mathcal{M}_{25}$/ $\mathcal{M}_{26}$	15 (III)/ 3 (I)	
1258 m	1253 vw	1247			$\nu(C\text{-}CH_3)/\nu_{III}(ring)$
1238 m-w	1237 w	1228			$\nu_{as}(N11C)/\nu_{III}(ring)/\delta_I(CH)$
1221 sh	1214 vw	1208			$\nu_{as}(CO)/\nu_{as}(N11C)/$ $\delta(C6H)/\nu_{III}(ring)$
	1206 vw	1205			$\delta(NH)/\delta_I(CH)/\rho(C15H_3)$
	1185 vw	1184			$\nu_{as}(CO)/\nu_{as}(N11C)/\delta_I(CH)$
1166 w	1166 vw	1165			$\gamma(O\text{-}CH_3)$
	1154 sh	1160			$\delta_I(CH)/\delta(NH)$
1109 w	1108 w	1116			$\delta_{III}(CH)/\delta(NH)/\delta(C\text{-}CH_3)$
1074 w	1069 vw	1084	$\mathcal{M}_{28}$	19b (III)	$\delta_I(CH)$
1026 w	1025 vw	1047			$\gamma(C\text{-}CH_3)$
977 m-w	977 w	980			$\rho(C14H_3)$
951 w	952 vw	947	$\mathcal{M}_{12}$	17a (III)	
924 w	915 vw	925	$\mathcal{M}_{12}$	17a (I)	
894 sh	894 vw	895			$\nu(C\text{-}CH_3)/\delta_{I,III}(ring)$
881 m-w	875 m	872			$\delta(N11C)/\delta_{III}(ring)$
837 vw	836 vw	835	$\mathcal{M}_{13}$	10a (III)	$\gamma_I(CH)$
803 vw	818 vw	802	$\mathcal{M}_{13}$	10a (I)	
775 m-w	776 m-w	775			$\delta_I(ring)/\delta(N11C)/\delta(COC)$
737 vw	746 w	737	$\mathcal{M}_{17}$	10b (I)	
	697 vw				
676 m-w	676 m-w	678	$\mathcal{M}_{29}$	6b (III)	$\delta_I(ring)/\delta(COC)$

663 w	659 vw	657	$\mathcal{M}_{29}$	6b (I)	$\delta(N11C)/\delta_{III}(ring)/\nu(C\text{-}CH_3)$
600 vw	601 vw	607			$\gamma(ring)/\gamma(NH)$
568 sh	570 vw	586			$\delta(COC)/\delta_{I,III}(ring)$
557 vw	553 vw	552	$\mathcal{M}_{11}$	6a (III)	$\delta_{I}(ring)$
528 vw	528 w	524			$\delta_{III}(ring)$
	501 vw	503			$\delta(COC)/\delta_{I,III}(ring)$
	447 vw	444	$\mathcal{M}_{19}$	16b (I)	$\gamma(NH)$
	381 w	388			
	329 sh	340		Skeletal vibrations	
	298 w	288			
	254 w	253			

[a] vw, very weak; w, weak; m, medium; s, strong; vs, very strong; sh, shoulder.

[b] ν, stretching; δ, in-plane bending; δ_{tw}, twist deformation; δ_{sc}, scissoring deformation; δ_{w}, wag deformation; γ, out-of-plane bending; ρ, rocking; s, symmetric; as, antisymmetric.

Table 3. Main experimental (SERS) and calculated Raman wavenumbers (cm^{-1}) of harmaline and assignments derived from the DFT calculations (B3LYP/6-31G**).

Raman wavenumber[a] / cm^{-1}			Assignments[b]		
SERS	FT-Raman	DFT (scaled)	Benzene modes		Other modes
			Gardner	Wilson	
1629 s	1625 w	1641			ν(C=N)
1599 sh	1604 vw	1633	$\mathcal{M}_{23}$	9b	ν(C=N)
1568 sh	1571 vw	1569	$\mathcal{M}_{4}$	9a	
1542 vs	1540 vs	1553			ν(C4=C12)
1515 sh	1515 vw	1508	$\mathcal{M}_{5}$	18a	ν(N11C)
1492 w	1471 w	1472			$\delta_{as}(C15H_3)$
1465 m		1442			$\delta_{s}(C15H_3)$
1437 m	1438 vw	1438			$\delta_{s}(C15H_3)/\delta_{as}(C14H_3)/\delta_{sc}(C2H_2)$
	1430 sh	1430	$\mathcal{M}_{24}$	18b	$\delta_{s}(C15H_3)/$ν(N11-C)
1372 s	1372 w	1374			$\delta_{s}(C14H_3)/\delta_{w}(C3H_2)/\nu_{III}$(ring)
	1362 sh	1366			$\delta_{s}(C14H_3)$
1335 vs	1334 vw	1348			ν_{I}(ring)/$\delta_{w}(CH_2)$/ν(N11C)
1313 sh	1301 w	1305	$\mathcal{M}_{26}$	3	ν(C4-C5)/$\delta_{tw}(C2H_2)$
1272 w	1273 vw	1259			ν(CO)/δ(NH)/ν(C12-C13)
1254 w	1247 vw	1238			$\delta_{tw}(C2H_2)$/δ(CH)
1236 sh	1230 vw	1220			$\delta_{tw}(C2H_2)/\delta_{w}(C3H_2)$/δ(CH)
1202 vw		1202			ν_{II}(ring)/ν(CO)/γ_{I}(CH)/ν(C-CH_3)
1171 w	1168 vw	1165			$\delta_{tw}(C3H_2)/\rho(C15H_3)$
1135 vw	1129 vw	1138	$\mathcal{M}_{27}$	14	
1106 sh	1079 sh	1085	$\mathcal{M}_{28}$	19b	ν_{III}(ring)/ν(O-CH_3)/ν(C-CH_3)
1076 m	1071 w	1084			$\rho(C14H_3)$/ν(N1-C2)
1036 vw	1038 vw	1059			$\rho(CH_2)/\delta(C14H_3)$/ν(O-$CH_3$)/ δ(CH)
	1021 vw	1035			$\delta(C14H_3)/\rho(CH_2)$
989 m	980 vw	979			$\rho(C14H_3)$/ν(C3-C2)
949 vw	938 vw	908			$\rho(C14H_3)$/δ(C3-C2-N)
906 vw	906 vw	899			ν(C-CH_3)/δ(C4-C3-C2)
859 w	857 vw	845			ν(C3-C2-N)/$\rho(C14H_3)$
	834 vw	834			γ(C9H)
805 vw	809 vw	801	$\mathcal{M}_{13}$	10a	
770 w	761 vw	773			$\delta_{I,II}$(ring)/$\rho(CH_2)$
750 sh	751 sh	747	$\mathcal{M}_{17}$	10b	
712 vw	709 vw	713			γ_{II}(ring)/γ_{I}(CH)
677 w	680 vw	694			γ_{III}(ring)
654 w	651 vw	646			δ(ring)
	369 vw	634	$\mathcal{M}_{18}$	4	

617 m	618 vw	628			$\delta(COC)/\delta_{III}(ring)/\nu(C\text{-}CH_3)$
573 vw	558 vw	572			$\delta(COC)/\delta_{II,III}(ring)$
553 vw	549 vw	548			$\gamma_{II,III}(ring)$
529 vw	533 vw	527	$\mathcal{M}_{29}$	6b	$\delta_{III}(ring)$
476 vw	492 vw	499			$\delta(COC)/\delta(N\text{-}C\text{-}CH_3)$
464 vw	460 vw	467			$\delta_{III}(ring)/\delta(COC)$
441 vw	439 vw	441	$\mathcal{M}_{19}$	16b	$\gamma(NH)$
377 vw	327 vw	327			
	302 vw	299		Skeletal vibrations	
	288 vw	269			

[a] vw, very weak; w, weak; m, medium; s, strong; vs, very strong; sh, shoulder.

[b] ν, stretching; δ, in-plane bending; δ_{tw}, twist deformation; δ_{sc}, scissoring deformation; δ_w, wag deformation; γ, out-of-plane bending; ρ, rocking; s, symmetric; as, antisymmetric.

Table 4. Main experimental (SERS) and calculated Raman wavenumbers (cm^{-1}) of harmalol and assignments derived from the DFT calculations (B3LYP/6-31G**).

Raman wavenumber[a] / cm^{-1}			Assignments[b]		
SERS	FT-Raman	DFT (scaled)	Benzene modes		Other modes
			Gardner	Wilson	
1615 sh	1635 m	1641			ν(C=N)/ν(C4=C12)
1600 m-w		1580	$\mathcal{M}_4$	9a	ν(N11C)/δ(OH)
1556 m-w	1559 s	1553			ν(C4=C12)
1514 vw	1517 sh	1517	$\mathcal{M}_5$	18a	ν(N11C)/ν(CO)/δ(OH)
1486 m	1469 w	1454			$\delta_{sc}(CH_2)$
		1451			$\delta_{as}(CH_3)$
1442 m-w	1442 w	1441			$\delta_{as}(CH_3)/\delta_{sc}(CH_2)$
	1430 sh	1434	$\mathcal{M}_{24}$	18b	ν(C3-C4)/ν(N11C)
1410 sh	1403 w	1372			$\delta_s(CH_3)/\delta_w(CH_2)$/δ(OH)/ ν(N11C)/ν(C3-C4)
1379 vw	1376 m	1363			$\delta_s(CH_3)$
1355 sh	1340 s	1329			$\delta_w(CH_2)$
1324 s	1312 sh	1321			ν(CO)/ν(N11C)/ν_{III}(ring)
	1295 m	1306	$\mathcal{M}_{26}$	3	$\delta_{tw}(CH_2)$
	1260 m	1258			δ(NH)/ν(CO)/ν(C12-C13)
1234 vw	1237 sh	1239			$\delta_{tw}(CH_2)$/δ(CH)
	1219 vw	1216			$\delta_{tw}(C2H_2)/\delta_w(C3H_2)$/δ(CH)
1190 vw	1195 vw	1206			δ(OH)/ν(CO)/ν_{II}(ring)
1174 vw	1180 vw	1181			δ(OH)/δ(NH)
	1162 sh	1164			$\delta_{tw}(CH_2)$
1137 vw	1141 vw	1140			δ(OH)/δ(NH)/δ(CH)
1076 w	1079 m	1082			δ_{II}(ring)/ν(C-CH_3)/ν(ring)
1039 vw	1039 vw	1035			$\delta_{as}(CH_3)/\rho(CH_2)$
986 w	996 m	980			ν(C3-C2)/$\rho(CH_3)$
	890 vw	901			ν(C-CH_3)/δ_{III}(ring)
	859 w	847			δ(N11C)/δ_{II}(ring)
815 vw		829			γ(C9H)
776 vw	776 m	781			ν(CO)/γ(C_7H)/$\delta_{I,II}$(ring)
	688 vw	694			γ_{III}(ring)
652 vw	655 m	650			δ(ring)
617 m	624 m	629	$\mathcal{M}_{18}$	4	γ(NH)/δ_{III}(ring)
557 vw	557 vw	553			$\gamma_{II,III}$(ring)
547 vw		542			δ_{II}(ring)
529 vw	533 vw	531	$\mathcal{M}_{29}$	6b	γ_{III}(ring)
475 vw	481 vw	485			δ_{III}(ring)
	447 vw	440	$\mathcal{M}_{19}$	16b	γ(NH)

378 vw	371 vw	347	Skeletal vibrations

[a] vw, very weak; w, weak; m, medium; s, strong; sh, shoulder.

[b] ν, stretching; δ, in-plane bending; δ_{tw}, twist deformation; δ_{sc}, scissoring deformation; δ_{w}, wagging deformation; γ, out-of-plane bending; ρ, rocking; s, symmetric; as, antisymmetric.

Figure Captions

Figure 1. Structure and numbering of the main components of Syrian Rue: (a) harmane, (b) harmine, (c) harmaline and (d) harmalol.

Figure 2. FT-Raman and DFT scaled calculated spectra of (a) harmane and (b) harmine.

Figure 3. FT-Raman and DFT scaled calculated spectra of (a) harmaline and (b) harmalol.

Figure 4. SERS and FT-Raman spectra of (a) harmane, (b) harmine and (c) harmaline. The SERS spectra were baselined corrected. The intensity was normalized to the band at (a) 978, (b) 977 and (c) 1171 cm^{-1}.

Figure 5. Adsorption mechanism of harmala, harmine and harmaline. The interaction takes place through the N atom in the pyridine ring. The molecule is tilted with respect to the Ag surface.

Figure 6. SERS and FT-Raman spectra of harmalol. The SERS spectrum was baselined corrected. The intensity was normalized to the band at 1442 cm^{-1}.

Figure 7. Adsorption mechanism of harmalol. The interaction takes place through the N atom in the pyridine ring and the OH in ring I. The molecule lies parallel to the Ag surface.

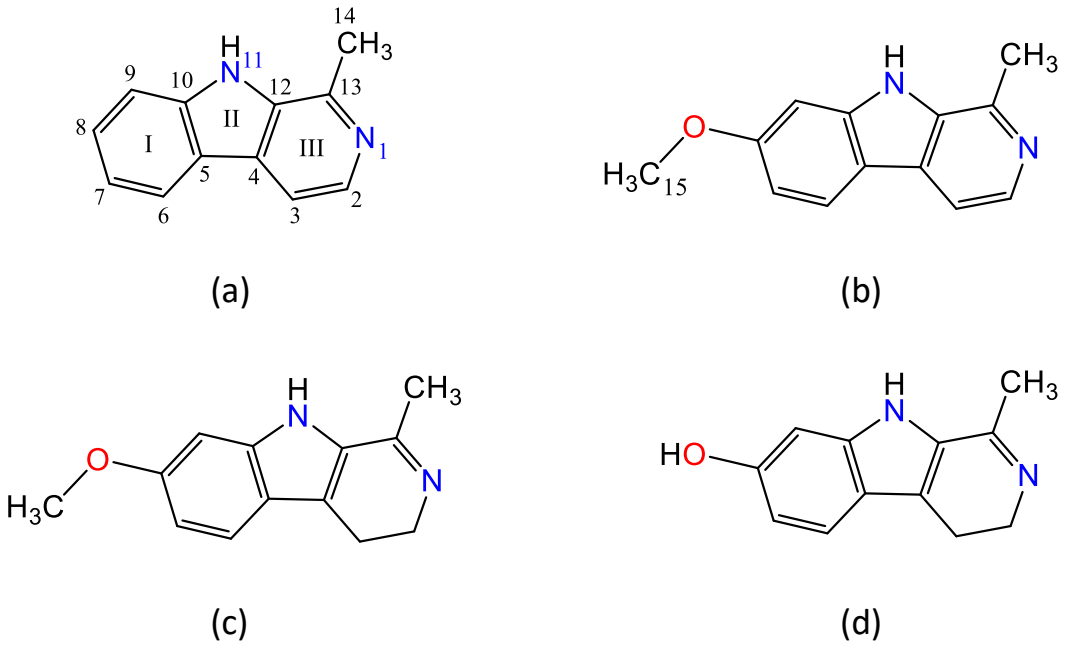

Figure 1. Structure and numbering of the main components of Syrian Rue: (a) harmane, (b) harmine, (c) harmaline and (d) harmalol.

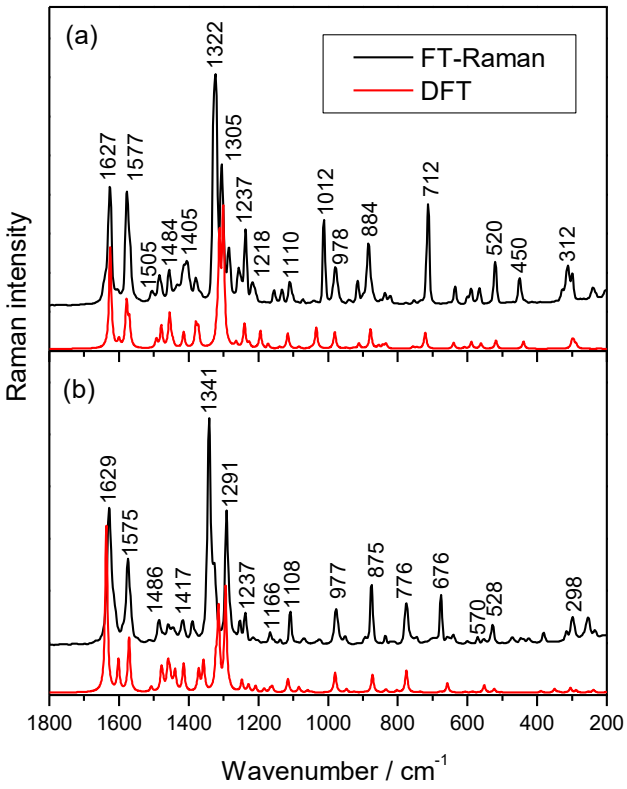

Figure 2. FT-Raman and DFT scaled calculated spectra of (a) harmane and (b) harmine.

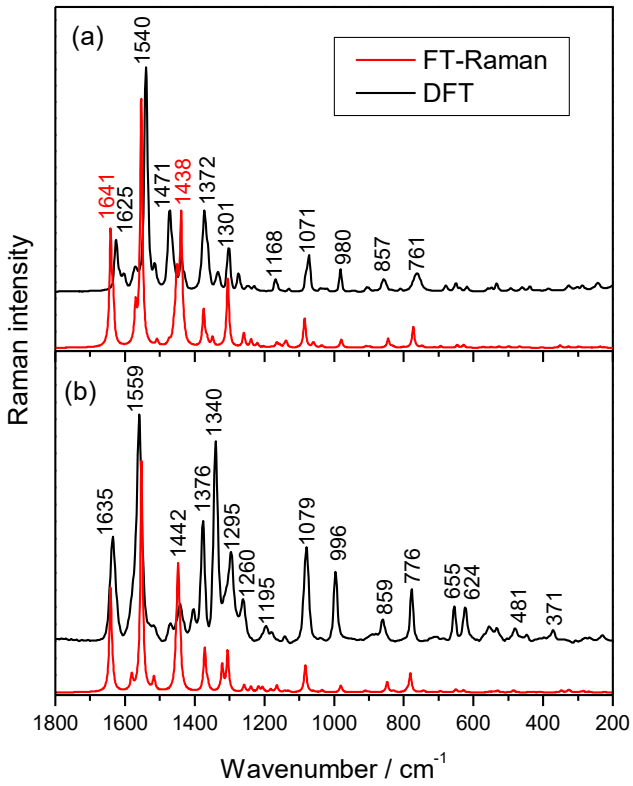

Figure 3. FT-Raman and DFT scaled calculated spectra of (a) harmaline and (b) harmalol.

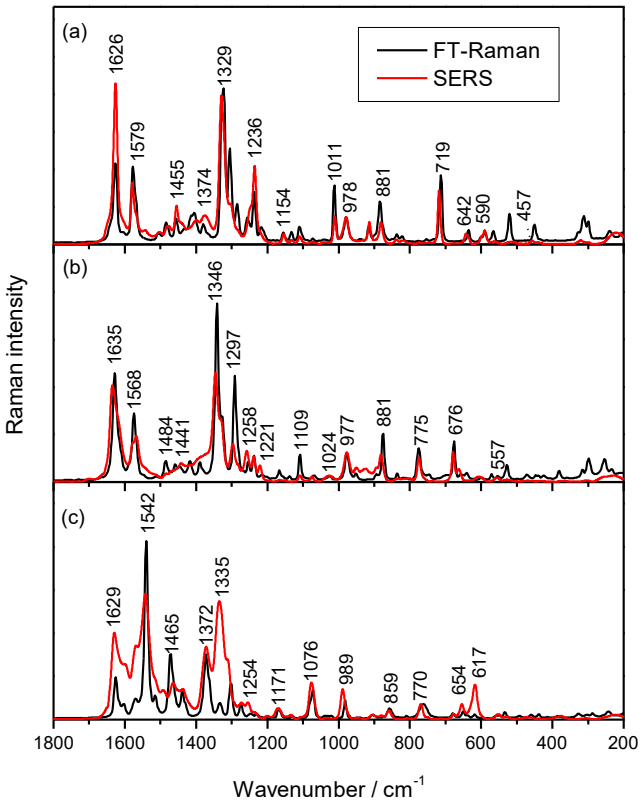

Figure 4. SERS and FT-Raman spectra of (a) harmane, (b) harmine and (c) harmaline. The SERS spectra were baselined corrected. The intensity was normalized to the band at (a) 978, (b) 977 and (c) 1171 cm^{-1}.

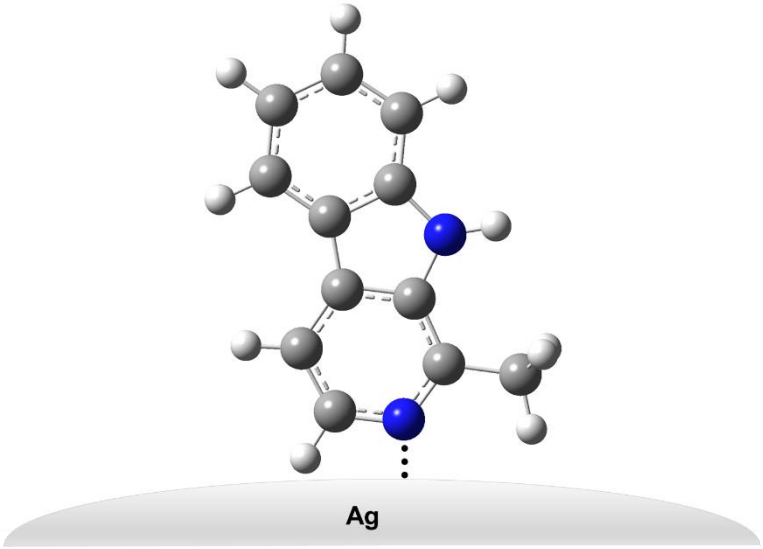

Figure 5. Adsorption mechanism of harmane, harmine and harmaline. The interaction takes place through the N atom in the pyridine ring. The molecule is tilted with respect to the Ag surface.

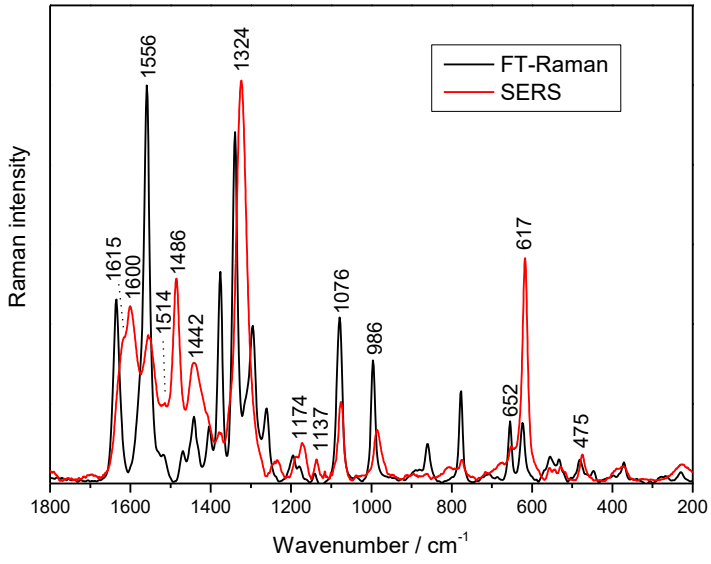

Figure 6. SERS and FT-Raman spectra of harmalol. The SERS spectrum was baselined corrected. The intensity was normalized to the band at 1442 cm^{-1}.

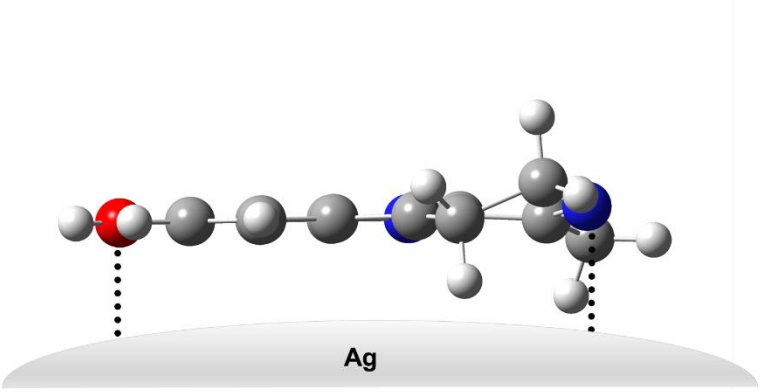

Figure 7. Adsorption mechanism of harmalol. The interaction takes place through the N atom in the pyridine ring and the OH in ring I. The molecule lies parallel to the Ag surface.